Journal of Applied Physics

RESEARCH ARTICLE | APRIL 18 2024

Deep selenium donors in $ZnGeP_2$ crystals: An electron paramagnetic resonance study of a nonlinear optical material

Special Collection: Defects in Semiconductors 2024

T. D. Gustafson; L. E. Halliburton; N. C. Giles; P. G. Schunemann; K. T. Zawilski; J. Jesenovec; K. L. Averett; J. E. Slagle

J. Appl. Phys. 135, 155704 (2024)
https://doi.org/10.1063/5.0205739

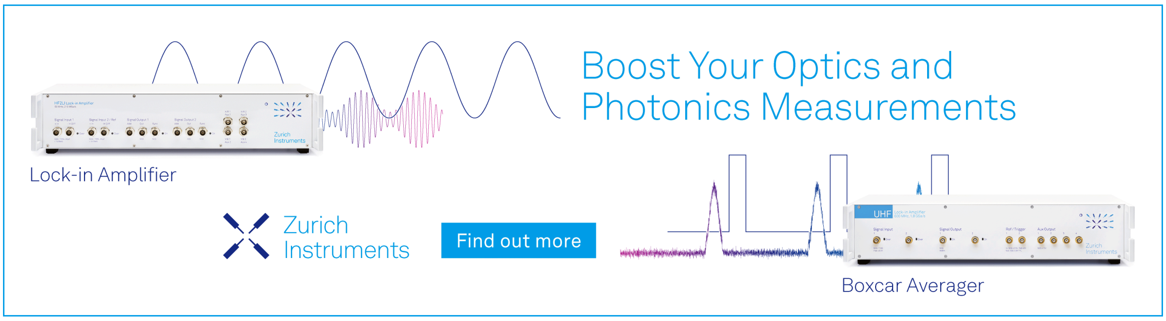

AIP Publishing

Journal of
Applied Physics

ARTICLE

pubs.aip.org/aip/jap

Deep selenium donors in $ZnGeP_2$ crystals: An electron paramagnetic resonance study of a nonlinear optical material

Cite as: J. Appl. Phys. **135**, 155704 (2024); doi: 10.1063/5.0205739
Submitted: 27 February 2024 · Accepted: 1 April 2024 ·
Published Online: 18 April 2024

View Online Export Citation CrossMark

T. D. Gustafson,[1,a)] L. E. Halliburton,[1,2,a)] N. C. Giles,[3] P. G. Schunemann,[4] K. T. Zawilski,[4] J. Jesenovec,[4] K. L. Averett,[5] and J. E. Slagle[5]

AFFILIATIONS

[1] Azimuth Corporation, 2970 Presidential Drive, Suite 200, Beavercreek, Ohio 45324, USA
[2] Department of Physics and Astronomy, West Virginia University, Morgantown, West Virginia 26506, USA
[3] Department of Engineering Physics, Air Force Institute of Technology, Wright-Patterson Air Force Base, Ohio 45433, USA
[4] BAE Systems, Nashua, New Hampshire 03061, USA
[5] Air Force Research Laboratory, Materials and Manufacturing Directorate, Wright-Patterson Air Force Base, Ohio 45433, USA

Note: This paper is part of the special topic, Defects in Semiconductors 2024.
[a)] **Authors to whom correspondence should be addressed:** Timothy.Gustafson@protonmail.com and Larry.Halliburton@mail.wvu.edu

ABSTRACT

Zinc germanium diphosphide ($ZnGeP_2$) is a ternary semiconductor best known for its nonlinear optical properties. A primary application is optical parametric oscillators operating in the mid-infrared region. Controlled donor doping provides a method to minimize the acceptor-related absorption bands that limit the output power of these devices. In the present study, a $ZnGeP_2$ crystal is doped with selenium during growth. Selenium substitutes for phosphorus and serves as a deep donor. Significant concentrations of native defects (zinc vacancies, germanium-on-zinc antisites, and phosphorous vacancies) are also present in the crystal. Electron paramagnetic resonance (EPR) is used to establish the atomic-level model for the neutral charge state of the selenium donor. The $S = 1/2$ signal from the neutral donors is produced at 6 K by illuminating with 633 nm light (electrons excited from doubly ionized Zn vacancies convert Se_P^+ donors to Se_P^0 donors). A **g** matrix, with principal values of 2.088, 2.203, and 1.904, is extracted from the angular dependence of the EPR spectrum. The principal-axis direction associated with the 1.904 principal value is close to a Se–Ge bond. This indicates an asymmetric distribution of unpaired spin density around the selenium ion and thus predicts the deep donor behavior.

I. INTRODUCTION

Zinc germanium diphosphide ($ZnGeP_2$ or simply ZGP) is a tetrahedrally bonded indirect-gap semiconductor (the conduction band is 1.99 eV above the highest valence band). These crystals are widely used in optical parametric oscillators (OPOs) to generate tunable coherent output at high power levels in the mid-infrared region.[1,2] Unfortunately, the performance of the OPOs is often adversely affected by unwanted optical absorption bands that overlap the pump and/or idler wavelengths. Native defects, unintentionally present in the $ZnGeP_2$ crystals, are responsible for the residual absorption bands. Singly ionized zinc vacancies (V_{Zn}^-) have been identified as the primary defect causing the dominant unwanted absorption.[3,4] Efforts to remove these vacancies during growth have yielded improved materials, but large concentrations of zinc vacancies still remain in many of the $ZnGeP_2$ crystals grown today. An alternative approach to minimizing the unwanted absorption is to use donor doping to place all the zinc vacancies in the doubly ionized charge state (V_{Zn}^{2-}). Absorption bands have not been associated with this latter charge state of the zinc vacancy. Sulfur and selenium, substituting for phosphorus, are candidates for controlled donor doping.[5]

In the present report, we use electron paramagnetic resonance (EPR) to identify and characterize neutral selenium donors in a

$ZnGeP_2$ crystal. Exposing a crystal doped with selenium to 633 nm light while being held at 6 K produces the EPR signal from neutral selenium donors. All the selenium donors are in the singly ionized charge state (Se_P^+) in the as-grown crystal (i.e., before light) and have no unpaired spins. The light converts these donors to the $S = 1/2$ neutral charge state (Se_P^0) by moving electrons from zinc vacancies to selenium. At 6 K, the neutral donors thermally decay in a few seconds after removing the light. A **g** matrix (principal values and principal-axis directions) is obtained from the angular dependence of the EPR spectrum. This matrix suggests that the donor's unpaired spin has an asymmetric distribution about the selenium ion, with considerable spin density near one adjacent germanium ion. As is usual for II-IV-P_2 crystals, EPR also reveals the presence of significant concentrations of native defects in the $ZnGeP_2$ sample.[6–22]

The present work indicates that the neutral selenium donor is deep, although not as deep as the neutral phosphorous vacancy. In the infrared absorption study of Giles *et al.*,[5] a band peaking near 0.3 eV (~4.1 μm) is assigned to the transition of an electron from a neutral selenium donor to the conduction band. For perspective, neutral selenium donors are hydrogenic in GaP, the III-V analog of $ZnGeP_2$.[23]

II. EXPERIMENTAL DETAILS

A selenium-doped $ZnGeP_2$ crystal was grown by the horizontal gradient freeze method at BAE Systems (Nashua, NH).[2,24] The presence of Se in the crystal was verified with x-ray fluorescence (XRF). A transparent furnace was used for growth and the starting materials were synthesized from high-purity elements. The Se doping level in the starting material was approximately 100 ppm (not all the Se may have entered the crystal). A small rectangular-shaped sample suitable for EPR experiments was cut from the larger boule. Its dimensions are $3.1 \times 3.1 \times 5.5\ mm^3$. The $ZnGeP_2$ crystals have a tetragonal structure (space group $I\bar{4}2d$) with $c = 10.71$ Å and $a = 5.46$ Å.[25] The *c* axis is the unique [001] direction and the two equivalent *a* axes are the [100] and [010] directions. Each zinc has four phosphorous neighbors, each germanium has four phosphorous neighbors, and each phosphorus has two zinc neighbors and two germanium neighbors. Figure 1 shows the phosphorous site (occupied by a selenium ion) and its four neighbors. References 18 and22 provide more complete descriptions of the $ZnGeP_2$ chalcopyrite structure.

EPR spectra were acquired with a Bruker EMX spectrometer operating near 9.375 GHz. An Oxford Instruments ESR-900 helium-gas flow system controlled the sample temperature. The native defects and the selenium donors were converted to paramagnetic charge states with 633 nm light from a He–Ne laser. Time-decay data were taken with the spectrometer operated in a kinetics mode (a time sweep with a fixed magnetic field corresponding to a peak in the EPR spectrum). Estimates of the concentrations of defects, with absolute values valid within a factor of two and relative values good to 10%, were obtained by comparing their spectra (intensities, linewidths, and number of lines) to a Bruker standard pitch sample.

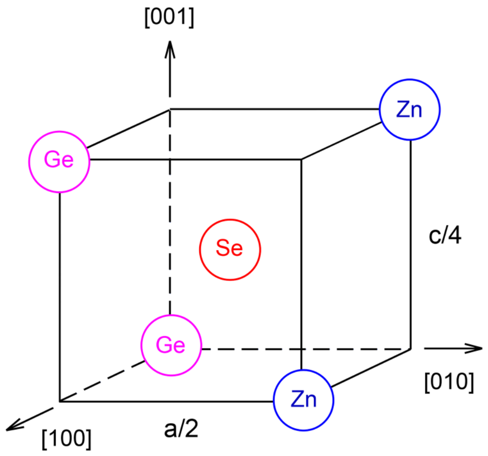

FIG. 1. Selenium on a phosphorous site in $ZnGeP_2$, with its two zinc neighbors and two germanium neighbors. The [001] direction is the unique *c* axis and the [100] and [010] directions, in the basal plane, are the two equivalent *a* axes.

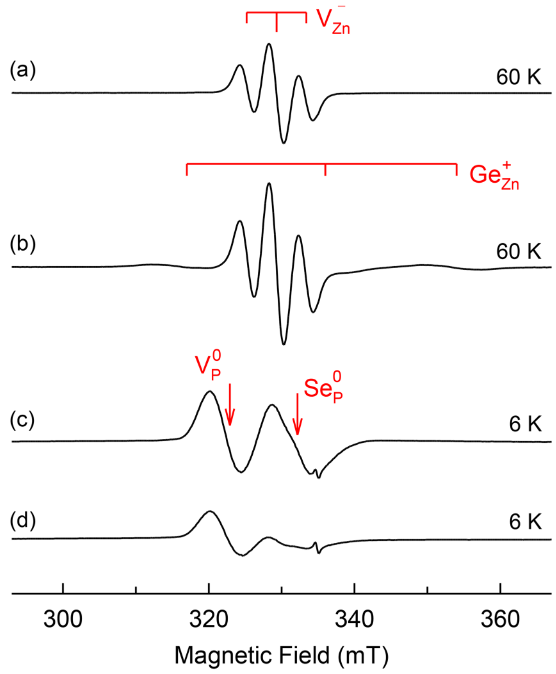

FIG. 2. EPR spectra acquired with the magnetic field along the *c* axis. (a) Spectrum taken at 60 K without light showing only the singly ionized zinc vacancy (V_{Zn}^-). (b) Spectrum taken at 60 K with 633 nm light showing the increase in the singly ionized zinc vacancy (V_{Zn}^-) and the appearance of the singly ionized germanium-on-zinc antisite (Ge_{Zn}^+). (c) Spectrum taken at 6 K with 633 nm light showing the neutral phosphorous vacancy (V_P^0) and neutral selenium donor (Se_P^0). (d) Spectrum taken at 6 K after removing the 633 nm light showing the neutral phosphorous vacancy donor (V_P^0) has decreased and the neutral selenium donor (Se_P^0) has disappeared.

III. EPR RESULTS

A. Native defects

Three native defects (one acceptor and two donors) are unintentionally present in the as-grown $\mathrm{ZnGeP_2}$ crystal. These are zinc vacancies, germanium-on-zinc antisites, and phosphorous vacancies.[6,7,10] The EPR spectrum in Fig. 2(a), taken at 60 K with the magnetic field along the *c* axis, shows that singly ionized zinc vacancies (V_{Zn}^{-}) are present in the as-grown crystal. This spectrum was obtained before an exposure to laser light. The 60 K temperature was chosen because it maximizes the V_{Zn}^{-} signal without introducing microwave power saturation effects. Doubly ionized zinc vacancies (V_{Zn}^{2-}) are also present in the as-grown crystal, as demonstrated by the subsequent increase of V_{Zn}^{-} vacancies during illumination. The doubly ionized zinc vacancies are not seen with EPR as they have no unpaired spins. There are three lines in the V_{Zn}^{-} spectrum, with relative intensities of 1:2:1, representing equal hyperfine interactions with two of the phosphorous ions adjacent to the vacancy.[6] In Fig. 2(a), the concentration of V_{Zn}^{-} acceptors is approximately $5.8 \times 10^{18}\ \mathrm{cm^{-3}}$.

The spectrum in Fig. 2(b) was then taken while the crystal was exposed to 633 nm light. These data were also acquired at 60 K with the magnetic field along the *c* axis. Spectrometer settings were the same in Figs. 2(a) and 2(b), so the two spectra can be directly compared. Signals from germanium-on-zinc antisite donors ($\mathrm{Ge_{Zn}^{+}}$) have appeared and the intensity of the V_{Zn}^{-} acceptor spectrum has increased. Before light, the antisites are doubly ionized ($\mathrm{Ge_{Zn}^{2+}}$). The 633 nm light moves electrons from zinc-vacancy acceptors to the doubly ionized germanium-on-zinc antisite donors, thus forming the paramagnetic $\mathrm{Ge_{Zn}^{+}}$ donors. As illustrated by the stick diagram, the $\mathrm{Ge_{Zn}^{+}}$ donor spectrum consists of three lines caused by equal hyperfine interactions with two of the phosphorous neighbors.[10] In Fig. 2(b), the concentrations of V_{Zn}^{-} acceptors and $\mathrm{Ge_{Zn}^{+}}$ donors are approximately 9.4×10^{18} and $6.2 \times 10^{18}\ \mathrm{cm^{-3}}$, respectively. The number of $\mathrm{Ge_{Zn}^{+}}$ donors formed is greater than the increase in V_{Zn}^{-} acceptors. This suggests that neutral zinc vacancies (V_{Zn}^{0}), with no unpaired spins, may also be produced during illumination.

Next, the crystal was cooled to 6 K and the spectrum in Fig. 2(c) was obtained while exposing the crystal to 633 nm light. A signal from neutral phosphorous-vacancy donors (V_{P}^{0}) is seen,[7] as well as the signal we assign to neutral selenium donors ($\mathrm{Se_{P}^{0}}$). The small sharp line near 334 mT is from the cryogenic glassware. The V_{Zn}^{-} acceptors and $\mathrm{Ge_{Zn}^{+}}$ donors observed at 60 K in Fig. 2(b), although present at 6 K, are severely saturated with microwave power at this lower temperature and do not make significant contributions to the EPR spectrum in Fig. 2(c). When the temperature is above 10 K, the V_{Zn}^{-} lines are much larger, and the underlying selenium donor line cannot be monitored. In Fig. 2(c), the concentrations of the V_{P}^{0} and $\mathrm{Se_{P}^{0}}$ donors are approximately 1.0×10^{18} and $1.7 \times 10^{18}\ \mathrm{cm^{-3}}$, respectively. The V_{P}^{0} linewidth is 4.5 mT and the $\mathrm{Se_{P}^{0}}$ linewidth is 6.1 mT.

Finally, the 633 nm light was removed and the spectrum in Fig. 2(d) was taken at 6 K after waiting 2 min with the sample in the dark. The neutral selenium donors decay completely in this time and the concentration of neutral phosphorous-vacancy donors is reduced to $0.6 \times 10^{18}\ \mathrm{cm^{-3}}$. A strongly saturated singly ionized zinc vacancy signal is seen near 330 mT in Fig. 2(d). Figure 3 shows the decay of the neutral selenium donor EPR spectrum at 6 K when the 633 nm light is removed (the magnetic field was fixed at 328.3 mT). For this sample, half of these neutral donors decay in approximately 2 s. The mechanisms responsible for the decay in Fig. 3 have not been established. Direct donor–acceptor recombination involving zinc-vacancy acceptors and selenium donors is likely, and crystals with different concentrations of native defects are expected to have different decay times for the neutral selenium donors when the light is removed.

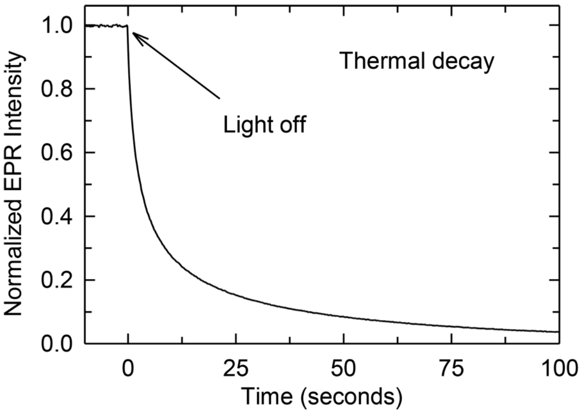

FIG. 3. Thermal decay of the neutral selenium donor ($\mathrm{Se_{P}^{0}}$) after removing the 633 nm light. These data were obtained by monitoring the intensity of the EPR signal at 6 K. The magnetic field, fixed at 328.3 mT, was along the *c* axis.

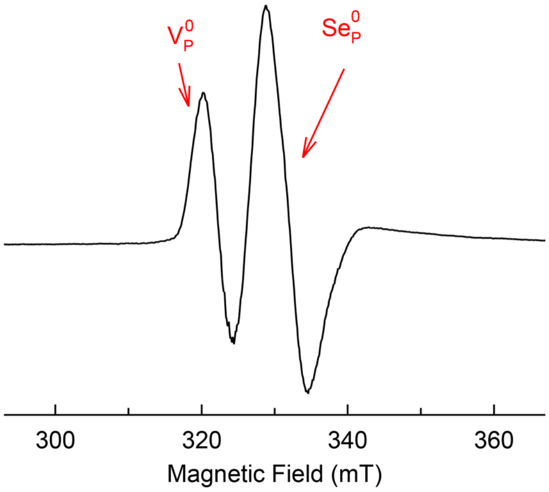

FIG. 4. Difference spectrum obtained by subtracting the spectrum taken after removing the 633 nm light from the spectrum taken with the light on. The temperature is 6 K and the magnetic field is along the *c* axis. In the difference spectrum, the intensity of the neutral selenium donor ($\mathrm{Se_{P}^{0}}$) is enhanced relative to the intensity of the neutral phosphorous vacancy (V_{P}^{0}).

B. Selenium donors

The **g** matrix of the neutral selenium donor (Se_P^0) was extracted from the angular dependence of its EPR spectrum. Because of interference from overlapping V_P^0 lines, difference spectra were used to generate the needed angular data. As an example, the *c* axis spectrum in Fig. 4 was produced by subtracting the "after-light" spectrum in Fig. 2(d) from the "light-on" spectrum in Fig. 2(c). This subtraction leaves the Se_P^0 signal as the larger contributor to the EPR spectrum in Fig. 4 (i.e., the V_P^0 signal has been reduced by approximately half). Difference spectra ("light-on" minus "after-light") were obtained at 6 K for various directions of the magnetic field, with the Se_P^0 lines always being larger than the V_P^0 lines. The Se_P^0 donor's angular dependence is shown in Fig. 5 for the rotation of the magnetic-field direction in the *c*–*a* plane. Although the effect was minimized, interference from V_P^0 lines still prevented precise measurements of the Se_P^0 lines at some of the angles. There are eight crystallographically equivalent orientations (or sites) for the Se_P^0 donor in the $\mathrm{ZnGeP_2}$ lattice. Degeneracies reduce this to four distinguishable sites in the *c*–*a* plane, thus explaining the four curves in Fig. 5. These sites arise because structurally identical defects can occur with different orientations within a crystal.[26] The **g** matrices for the different sites have identical principal values but different symmetry-related orientations of their principal axes.

An $S = 1/2$ spin-Hamiltonian with only an electron Zeeman term ($\mathrm{H} = \beta \mathbf{S} \cdot \mathbf{g} \cdot \mathbf{B}$) describes the Se_P^0 lines near $\mathrm{g} = 2.0$ (i.e., the 290–360 mT region). A least-squares fitting program was used to extract the six **g** matrix parameters from the angular dependence in Fig. 5. These are the three principal values and the three Euler angles describing the directions of the principal axes. The zyz convention, defined in the EasySpin EPR simulation program,[27,28] is used for the (α,β,γ) Euler angles. Input data for the fitting were the 22 experimental line positions in Fig. 5 and their corresponding microwave frequencies. Energy eigenvalues of the Hamiltonian were repeatedly calculated as the six parameters were systematically varied. In this iterative process, the predicted line positions (obtained from the eigenvalues) were compared to the measured line positions until a "best fit" was achieved.

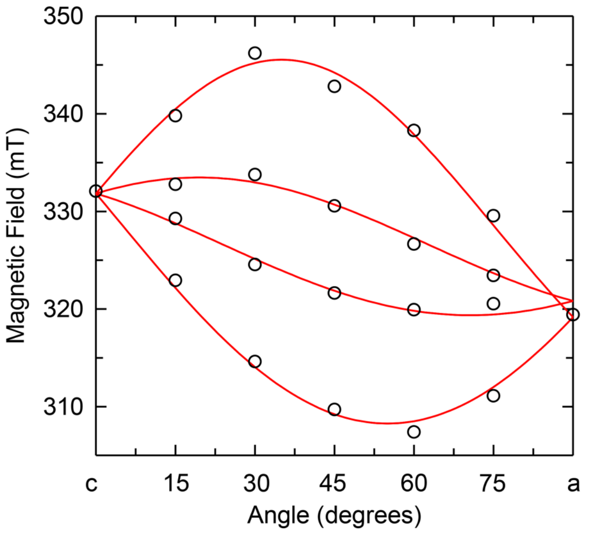

FIG. 5. Angular dependence of the EPR spectrum from the neutral selenium donor (Se_P^0). The discrete points are experimental data taken at 6 K with a microwave frequency of 9.375 GHz. The "best fit" parameters in Table I were used to generate the solid red lines.

Table I contains the final **g** matrix parameters for one orientation (or site) of the Se_P^0 donor. These parameters were used to generate the solid curves in Fig. 5. The directions of the principal axes for the other orientations are obtained by applying the crystal's symmetry elements. In Table I, the final Euler angles ($\alpha = 34.2°$, $\beta = 45.8$, and $\gamma = 32.3°$) have been converted to polar and azimuthal angles (θ and ϕ) to allow easier visualization of the principal directions. Here, θ is defined relative to the *c* axis and ϕ is defined as a rotation in the basal plane from [100] toward [010]. As demonstrated in the third and fourth rows in Table I, the principal direction associated with the g_3 principal value is near the bond joining a germanium ion to the selenium ion (on a phosphorous site). In Fig. 1, this is the bond between the lower-rear Ge ion and the Se ion. The small deviation of the principal direction of g_3 from the Ge–Se bond direction suggests that the second Ge adjacent to the Se ion may, to a much lesser degree, also share unpaired spin density.

It is reasonable to expect that a significant portion of the defect's unpaired spin density will be on a Ge ion adjacent to the Se ion. In an analysis of the polarities of ZnP and GeP bonds in $\mathrm{ZnGeP_2}$, Harrison[29] found that the effective charges of the Zn, Ge, and P ions are 0.60, 1.28, and −0.94, respectively. When these results are applied to the neutral selenium donor, the large positive effective charge of the Ge ions means that they will attract the donor electron more than the Zn ions and, thus, share the unpaired spin with the Se ion on the P site. Lattice relaxation may account for the preferential localization on one Ge neighbor. The relative amounts of spin density on the Ge and Se ions are not known, as there are no observable $^{77}\mathrm{Se}$ or $^{73}\mathrm{Ge}$ hyperfine lines. The neutral phosphorous vacancy is an example of another donor in $\mathrm{ZnGeP_2}$ having unpaired spin density on a neighboring germanium ion.[30]

TABLE I. The **g** matrix for the neutral selenium donor (Se_P^0) in $\mathrm{ZnGeP_2}$. Euler angles (α, β, γ) for the **g** matrix are 34.2°, 45.8°, and 32.3°, respectively [these angles are defined in Ref. 28]. In this table, polar and azimuthal angles (θ and ϕ) are used to describe the principal-axis directions. Uncertainties are estimated to be ±0.002 for the principal *g* values and ±2° for the angles. The fourth row is the Ge to P bond direction in the unrelaxed lattice.

	Principal values	Principal-axis directions θ (°)	Principal-axis directions ϕ (°)
g_1	2.088	127.3	76.4
g_2	2.203	67.5	148.0
g_3	1.904	45.8	34.2
Ge to P bond		54.8	44.0

IV. SUMMARY AND CONCLUSIONS

Neutral selenium donors (Se_P^0) are observed in a ZnGeP_2 crystal. The selenium ions occupy phosphorous sites and convert to paramagnetic neutral donors (Se_P^0) when the crystal is exposed at 6 K to 633 nm light. They return within seconds to the singly ionized state (Se_P^+) when light is removed. An anisotropic **g** matrix shows that selenium is a deep donor with a portion of the unpaired spin density on a neighboring Ge ion. This is consistent with infrared absorption results that place the neutral selenium donor approximately 0.3 eV below the conduction band.[5] Additional insights to the structure of the selenium donor may be obtained from experimental electron-nuclear double resonance (ENDOR) studies and from computational modeling studies.

Our investigation provides support for the use of controlled doping of ZnGeP_2 with selenium to minimize unwanted optical absorption from singly ionized zinc vacancies. This approach of controlled donor doping may also be relevant for minimizing unwanted optical absorption from singly ionized silicon vacancies (V_Si^-) in CdSiP_2,[19,21] another important II-IV-V_2 nonlinear optical material.

ACKNOWLEDGMENTS

Any opinions, findings, and conclusions or recommendations expressed in this paper are those of the authors and do not necessarily reflect the views of the United States Air Force.

AUTHOR DECLARATIONS

Conflict of Interest

The authors have no conflicts to disclose.

Author Contributions

T. D. Gustafson: Conceptualization (equal); Data curation (equal); Formal analysis (equal); Investigation (equal); Validation (lead); Writing – review & editing (equal). **L. E. Halliburton:** Conceptualization (equal); Data curation (equal); Formal analysis (equal); Writing – original draft (lead); Writing – review & editing (equal). **N. C. Giles:** Conceptualization (equal); Formal analysis (equal); Funding acquisition (equal); Investigation (equal); Resources (equal); Visualization (lead); Writing – review & editing (equal). **P. G. Schunemann:** Conceptualization (equal); Resources (equal); Writing – review & editing (equal). **K. T. Zawilski:** Conceptualization (equal); Resources (equal); Writing – review & editing (equal). **J. Jesenovec:** Conceptualization (equal); Writing – review & editing (equal). **K. L. Averett:** Conceptualization (equal); Funding acquisition (equal); Project administration (equal); Writing – review & editing (equal). **J. E. Slagle:** Conceptualization (equal); Funding acquisition (equal); Project administration (equal); Writing – review & editing (equal).

DATA AVAILABILITY

The data that support the findings of this study are available within the article.

REFERENCES

[1] V. Petrov, "Frequency down-conversion of solid-state laser sources to the mid-infrared spectral range using non-oxide nonlinear crystals," Prog. Quantum Electron. **42**, 1 (2015).

[2] P. G. Schunemann, K. T. Zawilski, L. A. Pomeranz, D. J. Creeden, and P. A. Budni, "Advances in nonlinear optical crystals for mid-infrared coherent sources," J. Opt. Soc. Am. B **33**, D36 (2016).

[3] S. D. Setzler, P. G. Schunemann, T. M. Pollak, M. C. Ohmer, J. T. Goldstein, F. K. Hopkins, K. T. Stevens, L. E. Halliburton, and N. C. Giles, "Characterization of defect-related optical absorption in ZnGeP_2," J. Appl. Phys. **86**, 6677 (1999).

[4] N. C. Giles, L. Bai, M. M. Chirila, N. Y. Garces, K. T. Stevens, P. G. Schunemann, S. D. Setzler, and T. M. Pollak, "Infrared absorption bands associated with native defects in ZnGeP_2," J. Appl. Phys. **93**, 8975 (2003).

[5] N. C. Giles, L. Bai, N. Y. Garces, T. M. Pollak, and P. G. Schunemann, "Assignment of infrared absorption bands in ZnGeP_2," Proc. SPIE **5337**, 11 (2004).

[6] M. H. Rakowsky, W. K. Kuhn, W. J. Lauderdale, L. E. Halliburton, G. J. Edwards, M. P. Scripsick, P. G. Schunemann, T. M. Pollak, M. C. Ohmer, and F. K. Hopkins, "Electron paramagnetic resonance study of a native acceptor in as-grown ZnGeP_2," Appl. Phys. Lett. **64**, 1615 (1994).

[7] N. C. Giles, L. E. Halliburton, P. G. Schunemann, and T. M. Pollak, "Photoinduced electron paramagnetic resonance of the phosphorus vacancy in ZnGeP_2," Appl. Phys. Lett. **66**, 1758 (1995).

[8] L. E. Halliburton, G. J. Edwards, M. P. Scripsick, M. H. Rakowsky, P. G. Schunemann, and T. M. Pollak, "Electron-nuclear double resonance of the zinc vacancy in ZnGeP_2," Appl. Phys. Lett. **66**, 2670 (1995).

[9] K. T. Stevens, S. D. Setzler, L. E. Halliburton, N. C. Fernelius, P. G. Schunemann, and T. M. Pollak, "Electron-nuclear double resonance study of the zinc vacancy in zinc germanium phosphide (ZnGeP_2)," Mater. Res. Soc. Symp. Proc. **484**, 549 (1997).

[10] S. D. Setzler, N. C. Giles, L. E. Halliburton, P. G. Schunemann, and T. M. Pollak, "Electron paramagnetic resonance of a cation antisite defect in ZnGeP_2," Appl. Phys. Lett. **74**, 1218 (1999).

[11] W. Gehlhoff, R. N. Pereira, D. Azamat, A. Hoffmann, and N. Dietz, "Energy levels of native defects in zinc germanium diphosphide," Phys. B **308–310**, 1015 (2001).

[12] W. Gehlhoff, D. Azamat, A. Hoffmann, and N. Dietz, "Structure and energy level of native defects in as-grown and electron-irradiated zinc germanium diphosphide studied by EPR and photo-EPR," J. Phys. Chem. Solids **64**, 1923 (2003).

[13] W. Gehlhoff, D. Azamat, and A. Hoffmann, "EPR studies of native and impurity-related defects in II-IV-V_2 semiconductors," Mater. Sci. Semicond. Process. **6**, 379 (2003).

[14] D. M. Hofmann, N. G. Romanov, W. Gehlhoff, D. Pfisterer, B. K. Meyer, D. Azamat, and A. Hoffmann, "Optically detected magnetic resonance experiments on native defects in ZnGeP_2," Phys. B **340–342**, 978 (2003).

[15] W. Gehlhoff and A. Hoffmann, "EPR identification of intrinsic and transition metal-related defects in ZnGeP_2 and other II-IV-V_2 compounds," Phys. B **404**, 4942 (2009).

[16] W. Gehlhoff, D. Azamat, A. Krtschil, A. Hoffmann, and A. Krost, "EPR and electrical studies of native point defects in ZnSiP_2 semiconductors," Phys. B **340–342**, 933 (2003).

[17] N. C. Giles, L. E. Halliburton, S. Yang, X. Yang, A. T. Brant, N. C. Fernelius, P. G. Schunemann, and K. T. Zawilski, "Optical and EPR study of point defects in CdSiP_2 crystals," J. Cryst. Growth **312**, 1133 (2010).

[18] E. M. Golden, N. C. Giles, E. Maniego, F. K. Hopkins, K. T. Zawilski, P. G. Schunemann, and L. E. Halliburton, "Identification of native defects (vacancies and antisites) in CdSiP_2 crystals," J. Appl. Phys. **118**, 185702 (2015).

[19] E. M. Scherrer, B. E. Kananen, E. M. Golden, F. K. Hopkins, K. T. Zawilski, P. G. Schunemann, L. E. Halliburton, and N. C. Giles, "Defect-related optical absorption bands in CdSiP_2 crystals," Opt. Mater. Express **7**, 658 (2017).

[20] E. M. Scherrer, L. E. Halliburton, E. M. Golden, K. T. Zawilski, P. G. Schunemann, F. K. Hopkins, K. L. Averett, and N. C. Giles, "Electron

paramagnetic resonance and optical absorption study of acceptors in $CdSiP_2$ crystals," AIP Adv. **8**, 095014 (2018).

[21] T. D. Gustafson, N. C. Giles, E. M. Scherrer, K. T. Zawilski, P. G. Schunemann, K. L. Averett, J. E. Slagle, and L. E. Halliburton, "Residual optical absorption from native defects in $CdSiP_2$ crystals," Opt. Mater. Express **14**, 293 (2024).

[22] T. D. Gustafson, N. C. Giles, P. G. Schunemann, K. T. Zawilski, K. L. Averett, J. E. Slagle, and L. E. Halliburton, "Intrinsic point defects (vacancies and antisites) in $CdGeP_2$ crystals," J. Appl. Phys. **133**, 245703 (2023).

[23] R. S. Title, "Paramagnetic-resonance studies of S, Se, and Te donor impurities in GaP," Phys. Rev. **154**, 668 (1967).

[24] K. T. Zawilski, P. G. Schunemann, T. M. Pollak, D. E. Zelmon, N. C. Fernilius, and F. K. Hopkins, "Growth and characterization of large $CdSiP_2$ single crystals," J. Cryst. Growth **312**, 1127 (2010).

[25] M. D. Lind and R. W. Grant, "Structural dependence of birefringence in the chalcopyrite structure: Refinement of the structural parameters of $ZnGeP_2$ and $ZnSiAs_2$," J. Chem. Phys. **58**, 357 (1973).

[26] J. A. Weil and J. R. Bolton, *Electron Paramagnetic Resonance: Elementary Theory and Practical Applications*, 2nd ed. (John Wiley & Sons, Hoboken, NJ, 2007), Chap. 4, pp. 96–97.

[27] S. Stoll and A. Schweiger, "Easyspin: A comprehensive software package for spectral simulation and analysis in EPR," J. Magn. Reson. **178**, 42 (2006).

[28] The EasySpin program is available at https://www.easyspin.org.

[29] W. A. Harrison, *Electronic Structure and the Properties of Solids* (W. H. Freeman and Company, San Francisco, 1980), Chap. 5, p. 130.

[30] X. Jiang, M. S. Miao, and W. R. L. Lambrecht, "Theoretical study of the phosphorus vacancy in $ZnGeP_2$," Phys. Rev. B **73**, 193203 (2006).